

## $A_{0.3}ZrNF_{1.3}$ Phases (A = Na, K) with Layered ZrNCl-Type Structures Prepared by Anion Metathesis

C. Stoltz,<sup>†</sup> K. Ramesha,<sup>†</sup> P. Piccoli,<sup>‡</sup> B. H. Toby,<sup>§</sup> and B. W. Eichhorn<sup>\*,†</sup>

Departments of Chemistry and Biochemistry and Geology, University of Maryland, College Park, Maryland 20742, and NIST Center for Neutron Research, National Institute of Standards and Technology, Gaithersburg, Maryland 20899-8563

Received May 13, 2005. Revised Manuscript Received July 20, 2005

$\beta$ -ZrNCl reacts with excess NaF in the solid state (350–400 °C) via anion exchange to give metastable  $Na_xZrNF_{1+x}$  ( $x \approx 0.3$ ), the first fluoride structural analogue of the MNX system (M = Zr, Hf; X = Cl, Br, I). The sodium-stabilized phase ( $P6_3/mmc$ ;  $a = 3.654(1)$  Å,  $c = 18.266(8)$  Å) was characterized by powder X-ray and neutron diffraction studies and was shown to contain successive  $FZr_2N_2F$  layers that are shifted from the original ZrNCl parent structure, giving a two-layer unit cell. Partially occupied Na and F sites create a stabilizing cluster effect between these layers. Heating the reaction mixture above 500 °C leads to the formation of the  $ZrN_xF_{4-3x}$  phase reported by Jung and Juza. Further heating results in decomposition to several known sodium fluorozirconate phases.

### Introduction

The MNX (M = Zr, Hf; X = Cl, Br, I) family of compounds shows interesting structural and physical properties that include superconductivity and optoelectronic capabilities.<sup>1–3</sup> These materials are lamellar, comprising M–N hexagonal nets in the  $a$ – $b$  plane (see Figure 1).<sup>4,5</sup> In the  $c$  direction, double layers of chloride ions are separated by a van der Waals gap and sandwich the double M–N layers. Depending on the group IV metal and the halide, the stacking sequences vary slightly, giving either the SmSI or YOF structure types.<sup>5,6</sup>

Materials properties in these and related systems often depend on the nature of the anion. Superconductivity has been the most widely studied feature of these materials, where a  $T_c$  of 25 K was found for Li-doped HfNCl.<sup>7,8</sup> Fluoride anions are especially well-known for dictating interesting and unusual properties, such as low phonon energies (relative to oxides), resistance to short-wavelength radiation, and low nonlinear refractive indices.<sup>9,10</sup> Although a ZrNCl-type fluoride analogue is unknown, a zirconium nitride fluoride phase,  $ZrN_xF_{4-3x}$ , has been reported by Jung

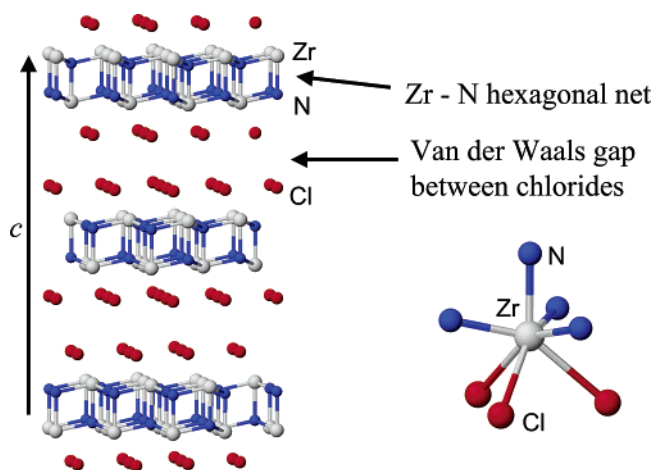


Figure 1. Ball-and-stick drawing of  $\beta$ -ZrNCl structure and Zr coordination sphere.

and Juza.<sup>11</sup> This phase is orthorhombic, having many superstructure modifications that vary with composition. One particular composition,  $ZrN_{0.906}F_{1.28}$ , was characterized having a 27-fold  $a$ -axis superstructure (space group  $Cm2a$ ) with a fluorite-type subcell. This fluorite-type cell is expected due to the tendency of N–F pairs to chemically and structurally resemble two  $O^{2-}$  units. Although this phase was synthesized by ammonolysis of  $ZrF_4$  at 580 °C, other studies claim that ammonolysis of  $\beta$ -ZrF<sub>4</sub> or  $ZrF_4 \cdot NH_3$  at similar temperatures yields  $Zr_4ON_3F_5$  and  $ZrNF$ , which is reported to be an isotype of baddeleyite,  $ZrO_2$ .<sup>12</sup> Subsequently, Schmid et al. thoroughly studied the fluoride and oxyfluoride phases<sup>13,14</sup> and describe the series as having an incommensurate, compositely modulated structure with variable composition.<sup>13</sup> Regardless,

<sup>†</sup> Department of Chemistry and Biochemistry, University of Maryland.

<sup>‡</sup> Department of Geology, University of Maryland.

<sup>§</sup> NIST.

- (1) Felsler, C.; Seshadri, R. *J. Mater. Chem.* **1999**, *9*, 459–464.
- (2) Zhu, L.; Ohashi, M.; Yamanaka, S. *Chem. Mater.* **2002**, *14*, 4517–4521.
- (3) Zhu, L.-P.; Ye, Z.-Z. *Huaxue Xuebao* **2003**, *61*, 1844–1848.
- (4) Ohashi, M.; Yamanaka, S.; Sumihara, M.; Hattori, M. *J. Solid State Chem.* **1988**, *75*, 99–104.
- (5) Chen, X.; Koizumi, T.; Yamanaka, S. *J. Phys.: Condens. Matter* **2002**, *14*, 11209–11212.
- (6) Ohashi, M.; Yamanaka, S.; Hattori, M. *Nippon Seramikkusu Kyokai Gakujutsu Ronbunshi* **1989**, *97*, 1181–1188.
- (7) Yamanaka, S. *Kotai Butsuri* **1998**, *33*, 711–716.
- (8) Yamanaka, S. *Annu. Rev. Mater. Sci.* **2000**, *30*, 53–82.
- (9) Martin, N.; Boutinaud, P.; Malinowski, M.; Mahiou, R.; Cousseins, J. C. *J. Alloys Compd.* **1998**, *275–277*, 304–306.
- (10) Burkhalter, R.; Dohnke, I.; Hulliger, J. *Prog. Cryst. Growth Charact. Mater.* **2001**, *42*, 1–64.

(11) Jung, W.; Juza, R. *Z. Anorg. Allg. Chem.* **1973**, *399*, 129–147.

(12) Schlichenmaier, R.; Schweda, E.; Straehle, J.; Vogt, T. *Z. Anorg. Allg. Chem.* **1993**, *619*, 367–373.

(13) Schmid, S.; Withers, R. L. *J. Solid State Chem.* **1994**, *109*, 391–400.

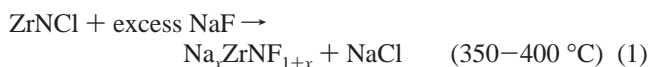
(14) Whithers, R. L.; Schmid, S.; Thompson, J. G. *Acta Crystallogr., Sect. B: Struct. Sci.* **1993**, *B49*, 941–951.

the reported ZrNF and oxynitride fluoride phases all have ZrO<sub>2</sub> or related structures. Importantly, none of these phases resemble the MNX lamellar phases where M = Hf, Zr and X = Cl, Br, I.

It is known that  $\beta$ -ZrNCl can be obtained by ammonolysis of ZrCl<sub>4</sub> at 300–400 °C followed by heating to 600 °C, as well as directly reacting Zr or ZrH<sub>2</sub> with sublimed NH<sub>4</sub>Cl.<sup>15,16</sup> However, these synthetic routes do not lead to the isostructural fluoride member of the MNX family. Rather, these methods lead to the Jung and Juza phases described above.<sup>11</sup> Previously, we reported a chloride-for-sulfide exchange via low-temperature, solid-state metathesis to give new sulfide derivative phases of ZrNCl. This topochemical method was shown to be a successful means to exchange the anions in this system without changing the parent host structure type.<sup>17</sup> Described herein is the topochemical synthesis of A<sub>0.3</sub>ZrNF<sub>1.3</sub> (A = Na, K) by anion exchange. This new sodium-stabilized zirconium nitride fluoride phase is the first fluoride material that retains the MNCl host structure type.

## Results

**Synthesis.** Recrystallized  $\beta$ -ZrNCl reacts with excess NaF at 350–400 °C for 10 days in vacuo with intermediate grinding, giving a sodium fluoride excess phase of formula Na<sub>x</sub>ZrNF<sub>1+x</sub> ( $x \approx 0.3$ ) according to eq 1.



Powder X-ray diffraction analysis of the reaction mixture shows that the reaction progresses via the depletion of the NaF reactant and the formation of the NaCl byproduct. The salt byproducts were removed by washing with distilled water, leaving the tan product, which was characterized by powder X-ray diffraction (XRD), energy-dispersive and wavelength-dispersive electron spectroscopy (EDS and WDS, respectively), transmission electron microscopy (TEM), and neutron powder diffraction studies. The product shows an expected hexagonal, lamellar ( $c = 18.27 \text{ \AA}$ ) structure type with  $P6_3/mmc$  crystal symmetry. EDX and WDS analyses give a Na:Zr ratio of 0.3–1.0, while WDS analysis shows a F:Zr ratio of 1.1–1.0. Assuming charge balance and an unchanged Zr:N ratio, we assign a compound formula of Na<sub>0.3</sub>ZrNF<sub>1.3</sub>. This result is consistent with the larger uncertainties in fluoride analysis<sup>18,19</sup> and the Rietveld results described in the next section. TEM images show 5–10 nm particles as well as expected [00 $l$ ] lattice fringes. The Na<sub>x</sub>-ZrNF<sub>1+x</sub> phase exists in a very narrow compositional range ( $x \approx 0.3$ ) as noted by compositional analysis of several independently synthesized batches of the material.

Above 500 °C, the washed Na<sub>x</sub>ZrNF<sub>1+x</sub> product slowly converts to a mixture of known sodium fluorozirconate phases (Na<sub>2</sub>ZrF<sub>6</sub>, Na<sub>3</sub>ZrF<sub>7</sub>) and zirconium nitride. When reaction 1 is conducted at lower temperatures or at 1:1 molar ratios of ZrNCl and NaF, only the sodium fluoride excess product and unreacted ZrNCl are present rather than mixed Cl/F phases. If the unwashed reaction mixture is allowed to reach higher temperatures (above 500 °C), the Jung and Juza phase is obtained. “As-prepared” ZrNCl (i.e., not recrystallized via vapor transport) is more poorly crystallized and has smaller particle sizes. This material undergoes the same reaction to give Na<sub>0.3</sub>ZrNF<sub>1.3</sub>, but at lower synthesis temperatures (275 °C), resulting in a much less crystalline product as seen in the XRD data (Supporting Information). The use of the as-prepared ZrNCl at reaction temperatures above 300 °C results in the Jung and Juza phase.

Similar reactions between excess KF and recrystallized ZrNCl give a less crystalline product. Multiple grinding and heating cycles at 275 °C appear to give K<sub>x</sub>ZrNF<sub>1+x</sub>. Powder XRD reveals the loss of KF and the concomitant formation of KCl. The salt byproducts were washed away with distilled water, as in the sodium fluoride case, leaving a dark green powder that has been characterized by powder XRD, EDS, and WDS. This compound is less crystalline than the sodium analogue, and structural analysis was not attempted. XRD analysis shows a lamellar structure with an increased interlayer  $d$  spacing ( $d \approx 9.75 \text{ \AA}$ ) relative to the sodium analogue ( $d \approx 9.13$ ) (see next section). EDX analysis provides an approximate 0.3–1.0 K:Zr ratio while WDS analysis gives a 1.1–1.0 F:Zr ratio, leading to an assigned formula of K<sub>0.3</sub>ZrNF<sub>1.3</sub>.

Upon heating the washed K<sub>0.3</sub>ZrNF<sub>1.3</sub> product above the reported reaction temperatures, known potassium fluorozirconate phases (K<sub>2</sub>ZrF<sub>6</sub>, K<sub>3</sub>ZrF<sub>7</sub>) begin to form. It is quite likely that these phases begin to form in the same temperature regime as the product, contributing to the structural/phase ambiguity. As was observed in the NaF reactions, lower temperatures or different stoichiometries only lead to unreacted starting materials and not to mixed Cl/F phases.

Reactions between ZrNCl and CsF gave unidentified products that did not appear to have the layered ZrNCl structure type (XRD analysis) and did not contain Cs (EDS analysis).

**Structural Studies.** Na<sub>0.3</sub>ZrNF<sub>1.3</sub>. The Na<sub>0.3</sub>ZrNF<sub>1.3</sub> phase has a double-layer hexagonal unit cell with  $P6_3/mmc$  crystal symmetry. Figure 2 shows the powder XRD profile and peak positions corresponding to refined lattice parameters  $a = 3.660(4) \text{ \AA}$  and  $c = 18.14(2) \text{ \AA}$  for the product made from recrystallized ZrNCl. This powder XRD profile is dominated by [00 $l$ ] reflections, due to severe preferred orientation in the powder sample, which is typical of ZrNCl-type compounds. The extreme preferred orientation, coupled with the poor sensitivity for scattering by N, F, and Na relative to Zr, prevented use of these data for Rietveld fitting. It should be noted that the [00 $l$ ] reflections do not shift upon washing with water, indicating that these materials do not intercalate water, as has been reported for other alkali-stabilized zirconium nitride chloride/sulfide materials.<sup>17</sup>

(15) Juza, R.; Friedrichsen, H. *Z. Anorg. Allg. Chem.* **1964**, *332*, 173–178.

(16) Ohashi, M.; Yamanaka, S.; Hattori, M. *J. Solid State Chem.* **1988**, *77*, 342–347.

(17) Stoltz, C.; Ramesha, K.; Sirchio, S. A.; Goenen, Z. S.; Eichhorn, B. W.; Salamanca-Riba, L.; Gopalakrishnan, J. *J. Am. Chem. Soc.* **2003**, *125*, 4285–4292.

(18) Tikhonravov, A. V.; Trubetskov, M. K.; Amotchkina, T. V.; Tikhonravov, A. A.; Ristau, D.; Gunster, S. *Proc. SPIE—Int. Soc. Opt. Eng.* **2003**, *5188*, 331–342.

(19) Kashin, G. N.; Makhnjuk, V. I.; Rumjantseva, S. M.; Shchekochihin, J. M. *Appl. Surf. Sci.* **1993**, *70–71*, 85–88.

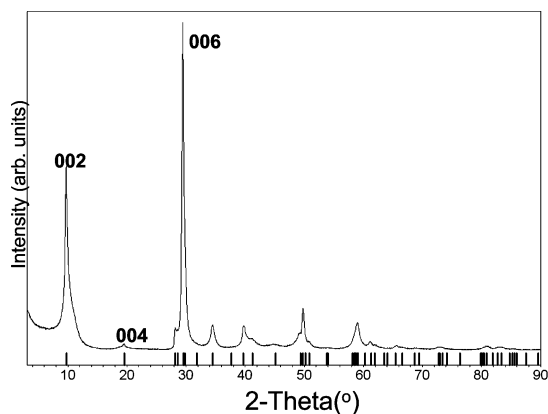


**Figure 2.** Powder XRD profile for Na<sub>x</sub>ZrNF<sub>1+x</sub> with selected [00*l*] reflections labeled. The tick marks represent calculated Bragg reflections associated with the refined unit cell.

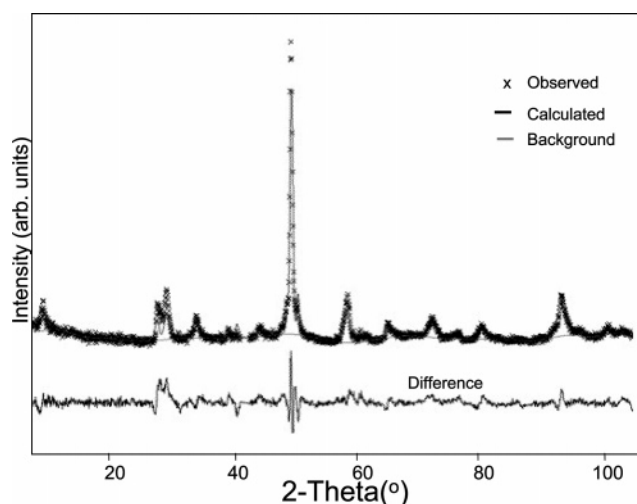


**Figure 3.** Observed, calculated, background, and difference powder neutron diffraction profiles (Rietveld analysis, GSAS) for Na<sub>0.3</sub>ZrNF<sub>1.3</sub>.

Full Rietveld structural analysis was performed using neutron diffraction data. Figure 3 shows calculated, observed, background, and difference neutron diffraction profiles. Table 1 provides the resulting structural model and Table 2 lists selected bond distances and angles. An idealized ball-and-stick structural drawing of the refined structure is given in Figure 4.

The space group was assigned from both XRD and neutron data by careful comparisons of fits to several possible unit cells and space groups with the Jade and GSAS software packages. Several models were constructed and refined in three different space groups, *P6<sub>3</sub>/mmc*, *R $\bar{3}m$* , and *P $\bar{3}m1$* , that most closely fit the observed systematic absences and structural motif of the system. The *P6<sub>3</sub>/mmc* space group and reported structural model were chosen because they had the best agreement with the experimental data. The models were refined independently from neutron and XRD data giving similar results. Both cells (XRD and neutron) are given in Table 1 for comparison.

The best structural model was based on the Zr<sub>2</sub>N<sub>2</sub> double layers of ZrNCl, shifted to give a two-layer unit cell. While these layers are well-defined, the positions of the interlayer sodium and fluoride atoms are less clear due to partial site occupancies and possible disorder. Candidate sites for interlayer Na and F atoms were found by examination of

**Table 1.** Neutron Diffraction Rietveld Refinement Data

diffraction data	neutron	X-ray
refinement type	Rietveld	unit cell
crystal system	hexagonal	hexagonal
space group	<i>P6<sub>3</sub>/mmc</i>	<i>P6<sub>3</sub>/mmc</i>
<i>a</i> /Å	3.654(1)	3.660(4)
<i>c</i> /Å	18.266(8)	18.14(2)
preferred orientation	0 0 1	
ESD of fit		0.055
$\chi^2$	3.628	
<i>R</i> <sub>wp</sub>	0.0998	
<i>R</i> <sub>p</sub>	0.0795	
Na		
<i>x</i>	1/3	
<i>y</i>	2/3	
<i>z</i>	0.703(4)	
<i>B</i> <sub>eq</sub>	0.001(1)	
occupied	0.3	
Zr		
<i>x</i>	1/3	
<i>y</i>	2/3	
<i>z</i>	0.435(1)	
<i>B</i> <sub>eq</sub>	0.036(4)	
occupied	1	
N		
<i>x</i>	1/3	
<i>y</i>	2/3	
<i>z</i>	0.9384(7)	
<i>B</i> <sub>eq</sub>	0.020(2)	
occupied	1	
F(1)		
<i>x</i>	0	
<i>y</i>	0	
<i>z</i>	0.3729(9)	
<i>B</i> <sub>eq</sub>	0.064(4)	
occupied	1	
F(2)		
<i>x</i>	2/3	
<i>y</i>	1/3	
<i>z</i>	1/4	
<i>B</i> <sub>eq</sub>	0.005(1)	
occupied	0.6	

**Table 2.** Selected Bond Lengths (Å) and Angles (deg)

Zr–N	2.112(1)
Zr–N	2.30(2)
Zr–F(1)	2.40(1)
Na–F(1)	2.52(4)
Na–F(2)	2.28(3)
N–Zr–N	119.9(1)
N–Zr–N	88.6(7)
Zr–F(1)–Zr	99.1(7)
F–Na–F(2)	79.7(4)
F(2)–Na–F(2)	107(2)

successive difference Fourier maps and then with the use of chemical intuition to assign plausible structures. Many arrangements were tested and gave reasonable fits; the presented model is the only plausible one we could find with respect to the resulting bond distances and bond valence analysis. The model presented here places an additional fluoride layer directly between the consecutive F–Zr<sub>2</sub>N<sub>2</sub>–F layers with sodium ions in octahedral holes. Alternate structural models with NaF<sub>5</sub> trigonal bipyramidal units in between the F–Zr<sub>2</sub>N<sub>2</sub>–F host or with sodium in the same plane as the F(2) layer, giving rise to a pseudo 9-coordinate sodium coordination sphere, produced implausible results. We speculate that the Na<sup>+</sup> and F<sup>–</sup> ions likely cluster<sup>20,21</sup> to

(20) Gektin, A. V.; Smushkova, V. I.; Shiran, N. V. *Opt. Spektrosk.* **1987**, *63*, 314–317.

(21) Cook, J. S.; Dryden, J. S. *J. Phys. C: Solid State Phys.* **1981**, *14*, 1133–1136.

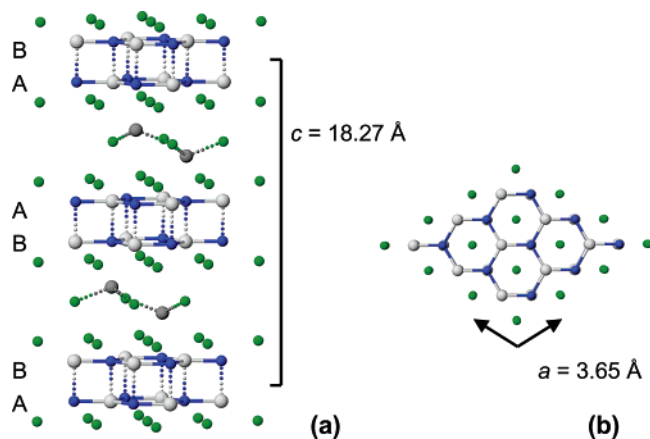


**Figure 4.** Ball-and-stick drawing of layered  $\text{Na}_x\text{ZrNF}_{1+x}$  structure perpendicular (a) and normal (b) to [001] zone axis. Selected Na sites have been removed for clarity. The color scheme is as follows: zirconium, gray; nitrogen, blue; sodium, dark gray; fluoride, green.

**Table 3. Bond Valence Calculation Values**

atom	coord sphere	bond valence
Zr	$\text{ZrN}_4\text{F}_3$	4.2
Na	$\text{NaF}_6$	0.9
Na	$\text{NaNF}_6$	1.07
Na	$\text{NaNF}_5$	0.87

maximize Na coordination and that the model presented here represents an average of many slightly different configurations. Occupancies of these atoms were fixed to match the chemical analysis data.

Bond valence calculations were carried out using the method of O'Keefe and Brese and are summarized in Table 3.<sup>22,23</sup> Note that the zirconium coordination sphere gives a bond valence of  $V_{\text{Zr}} = 4.2$ , which is in good agreement to the expected oxidation state of +4. The sodium bond valence depends on the choice of atoms included in the computation. Using only the nearest six F atoms and ignoring the partial occupancies, we obtain a bond valence of  $V_{\text{Na}} = 0.90$  for the  $\text{NaF}_6$  octahedron. Including the next-nearest neighbor N atoms boosts the bond valence to  $V_{\text{Na}} = 1.07$ . In the case where the interlayer fluoride site is not occupied, we compute  $V_{\text{Na}} = 0.87$  for a  $\text{NaNF}_5$  coordination sphere. This analysis supports our conjecture that the extra interlayer Na and F ions form clusters that optimize Na coordination and is consistent with analytical data and the structural refinements. This vacancy-clustering phenomenon is common in many metal halide materials.<sup>20,21</sup>

A March-Dollase preferred orientation correction along the [001] vector was needed to improve the Rietveld fit. The preferred orientation, which is strong in the case of X-rays and less significant for neutrons, is expected due to the thin, approximately 7 nm hexagonal platelike particles seen in the TEM images (Figure 5). The TEM lattice images (Figure 6) shows the appropriate  $\sim 9 \text{ \AA}$  interlayer spacing, in agreement with the diffraction results and proposed structural models.

Minor discrepancies between the calculated and observed profiles are seen, especially in the region just before  $30^\circ 2\theta$ . However, the overall fit is quite good considering the very

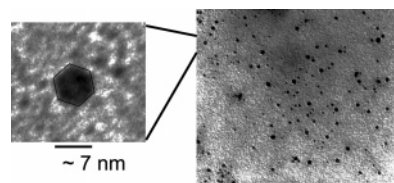


**Figure 5.** Bright-field TEM image of  $\text{Na}_x\text{ZrNF}_{1+x}$  with expanded area showing the approximate 7 nm particle size (hexagon outline drawn for clarity).

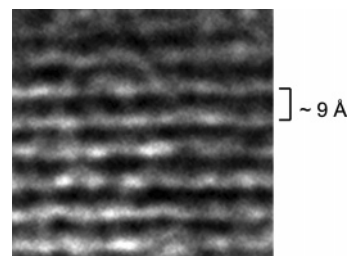


**Figure 6.** TEM image of  $\text{Na}_x\text{ZrNF}_{1+x}$  showing the appropriate interlayer spacing.

poor crystallinity of the sample and the complexities of the intralayer coordination.

The  $\text{Na}_x\text{ZrNF}_{1+x}$  structure is similar to that of  $\beta\text{-ZrNCl}$  (refer to Figures 1 and 4 for comparison). A slight  $a/b$  layer shift changes the ZrN layer stacking to an  $\text{AB}\cdots\text{BA}\cdots\text{AB}$  stacking sequence, giving a two-layer repeat unit as opposed to the three-layer repeat unit in  $\text{ZrNCl}$ . As in the  $\text{ZrNCl}$  structure, three fluorides are bound to each zirconium, giving sequential  $\text{F}-\text{Zr}_2\text{N}_2-\text{F}$  layers (directly replacing the chlorides of  $\text{ZrNCl}$ ). Between these layers, extra sodium and fluoride ions reside in partially occupied sites as shown in Figure 4. These sodium sites occupy pseudooctahedral holes between sequential fluoride layers. If the extra fluoride layer sites were fully occupied, each Na would have a pseudooctahedral  $\text{NaF}_6$  coordination sphere as shown in Figure S-1 (see Supporting Information).

The refined  $\text{Zr}-\text{F}$  (2.4  $\text{\AA}$ ) and  $\text{Na}-\text{F}$  (2.28  $\text{\AA}$ ) distances are similar to those in zirconium fluoride materials and known sodium fluorozirconates, while the 2.52  $\text{\AA}$   $\text{Na}-\text{F}$  distance seems slightly long in this coordination.<sup>12,24</sup>

As described in the previous section, an amorphous  $\text{Na}_x\text{ZrNF}_{1+x}$  phase is obtained from "as-prepared"  $\text{ZrNCl}$  according to eq 1. This amorphous material is not amenable to crystallographic analysis. Figure S-2 (see Supporting Information) displays the amorphous nature of the unwashed product obtained from "as-prepared"  $\text{ZrNCl}$  starting material and shows reflections for the  $\text{NaCl}$  byproduct and unwashed  $\text{NaF}$ .

$\text{K}_{0.3}\text{ZrNF}_{1.3}$ . The  $\text{K}_{0.3}\text{ZrNF}_{1.3}$  phase appears to be a structural analogue of the  $\text{Na}_{0.3}\text{ZrNF}_{1.3}$  phase, based on the similarity of the XRD patterns (Figure 7) and the common increase in the  $c$  lattice parameter (9.75  $\text{\AA}$ ) estimated from prominent powder X-ray diffraction [001] reflections. Although structural analysis is not possible due to poor crystallinity, we infer that the lamellar structure is retained. We can thus make structural estimates using the same fractional coordinates as in the sodium analogue. Retaining

(22) Brese, N. E.; O'Keefe, M. *Acta Crystallogr., Sect. B: Struct. Sci.* **1991**, *B47*, 192–197.

(23) O'Keefe, M.; Brese, N. E. *J. Am. Chem. Soc.* **1991**, *113*, 3226–3229.

(24) Ross, K. C.; Mitchell, R. H.; Chakhmouradian, A. R. *J. Solid State Chem.* **2003**, *172*, 95–101.

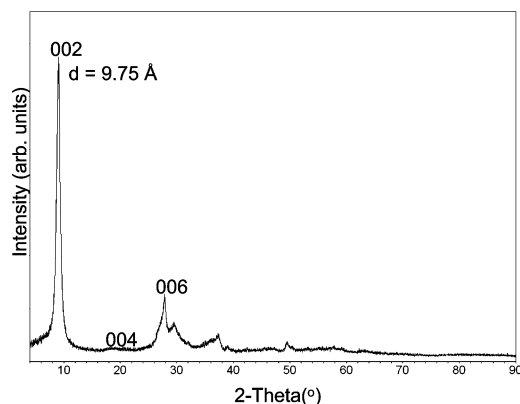


**Figure 7.** Powder XRD profile of K<sub>0.3</sub>ZrNF<sub>1.3</sub> showing the increased low-angle [00l] reflection.

the Zr–N and Zr–F bond distances from Na<sub>0.3</sub>ZrNF<sub>1.3</sub> and expanding the unit cell *c* lattice parameter (value obtained from powder XRD) lead to K–F distances of 2.34 and 2.63 Å within the structure, which are reasonable when considering the multiatom coordination sphere. Bond valence analysis using these calculated bond lengths provides bond valence values of 0.8 (KF<sub>6</sub>), 1.1 (KNF<sub>6</sub>), and 0.9 (KNF<sub>5</sub>). As in the sodium case, these values indicate the likelihood of clustering<sup>20,21</sup> to maintain an alkali bond valence close to 1.

### Discussion

Cation metathesis has become a well-known topochemical method for materials design, especially in solid-state oxide chemistry.<sup>25–27</sup> Cations can be exchanged in and out of inorganic hosts, having little or no effect on the bulk material properties.<sup>28</sup> Conversely, anions often account for many of the structural and physical properties of a material. For example, the structural type and stacking sequence of the MNX family (M = Zr, Hf; X = I, Br, Cl, F) depend mostly on the anion present in the host.<sup>5,6</sup> Another interesting example is given by the *T<sub>c</sub>* anion dependence in the superconducting molybdenum chalcogenide materials.<sup>29–31</sup> Although motivation for this work included the possibility of a superconducting MNX fluoride analogue, attempts at inducing superconductivity upon electron doping were unsuccessful.

Notably, a topochemical method such as anion metathesis was necessary to obtain a fluoride analogue to the MNX family that traditional synthetic methods could not provide. Although ZrNF (with the ZrNCl structure) was the target phase, it was not accessible without an AF (A = Na, K) intercalant. It appears that the excess, interlayer alkali fluoride plays a major role in stabilizing this structure. An interesting

comparison can be made with the A<sub>x</sub>Zr<sub>2</sub>N<sub>2</sub>SCl<sub>x</sub> compounds (A = Na, K, Rb).<sup>17</sup> The alkali chloride intercalated Zr<sub>2</sub>N<sub>2</sub>S phases do not achieve complete, stoichiometric loading of ACl, which is similar to the fluoride materials reported here. Although the exact reasons for the nonstoichiometric loading are unclear, it is possible that, in both cases, this incomplete intercalation phenomenon is a product of the synthetic methodology. While the low-temperature methods described here are sufficient for the anion exchange to take place, it is possible that more extreme conditions are necessary to achieve complete intercalation with this type of synthesis. However, more extreme reaction conditions lead to undesired high-temperature products in the fluoride materials, whereas alternative high-temperature methods in the sulfide series yield fully loaded stoichiometric phases (e.g., NaZr<sub>2</sub>N<sub>2</sub>SCl).<sup>17</sup>

It is not clear why pure ZrNF is not accessible by the methods described here. However, since fluoride is such a highly electronegative anion, interlayer cations may be necessary to maintain the layered structure. In contrast to the X···X van der Waals interactions in the other ZrNX phases (X = I, Br, Cl), the F–F repulsions in a putative ZrNF phase are possibly too large and require intercalated Na<sup>+</sup> ions to mediate the repulsion. One might expect that sodium can go into the layered structure because of its small size and that larger cations (e.g., cesium) should give alkali-free, layered ZrNF. However, as shown here, this is not the case. The stability of these kinetically stable fluoride MNX analogues likely relies on a balance between interlayer cation stabilization and small cation size.

The methods described here are necessary for the preparation of such materials; however, these synthetic conditions tend to provide poor crystallinity. The structural analysis, specifically the Rietveld refinement, proved to be a complicated task that required both XRD and neutron diffraction analyses. The possibility of a very small amount of oxide contamination also exists in the phases reported here. Fluoride readily reacts at elevated temperatures with glass, such as the tubes used in these experiments. Although no sign of glass etching was evident, it is possible that some of the fluoride sites are occupied by oxides, which could further explain the minor discrepancies in the WDS data. This contamination could also impact the Rietveld refinement results, decreasing the quality of the fit.

### Conclusion

We have prepared the first fluoride structural derivatives of the MNX family (M = Zr, Hf; X = Cl, Br, I). Solid-state anion metathesis reactions between ZrNCl and NaF at 350–400 °C give Na<sub>0.3</sub>ZrNF<sub>1.3</sub>, which retains the two-dimensional Zr–N host matrix. Similar reactions between ZrNCl and KF at 275 °C give a less crystalline, potassium analogue of this phase. Interestingly, while traditional (ammonolysis) synthetic routes fail to provide these fluoride materials, the solid-state anion-exchange methods described here are successful. Importantly, this chemistry illustrates the effectiveness of such nontraditional methods as pathways to new materials.

### Experimental Section

**General.** A nitrogen-filled Vacuum Atmospheres glovebox was utilized for storage and handling of air- and moisture-sensitive

- (25) Mandal, T. K.; Gopalakrishnan, J. *J. Mater. Chem.* **2004**, *14*, 1273–1280.  
 (26) Schaak, R.; Mallouk, T. *Chem. Mater.* **2002**, *14*, 1455–1469.  
 (27) Sivakumar, T.; Ramesha, K.; Lofland, S. E.; Ramanujachary, K. V.; Subbanna, G. N.; Gopalakrishnan, J. *Inorg. Chem.* **2004**, *43*, 1857–1864.  
 (28) Gopalakrishnan, J. *Chem. Mater.* **1995**, *7*, 1265–1275.  
 (29) Belin, S.; Burel, L.; Chevrel, R.; Sergent, M. *Mater. Res. Bull.* **2000**, *35*, 151–168.  
 (30) Mandal, K. C.; Savadogo, O. *Jpn. J. Appl. Phys., Part 1* **1991**, *30*, 3484–3487.  
 (31) Rao, G. V. S.; Shafer, M. W.; Kawarazaki, S.; Toxen, A. M. *J. Solid State Chem.* **1974**, *9*, 323–329.

materials. A high vacuum line ( $10^{-5}$  Torr) used for all glass tube evacuation consisted of a belt-driven mechanical pump followed by a glass oil diffusion pump and a liquid nitrogen trap. Evacuated silica tubes were sealed using an oxygen/hydrogen torch.

**Synthesis.**  $\beta$ -ZrNCl was prepared by flowing sublimed  $\text{NH}_4\text{Cl}$  over Zr metal (99.7% Cerac, 325 mesh) in an argon flow through furnace as previously reported.<sup>4,17</sup> Recrystallized ZrNCl (Figure S-3, Supporting Information) was prepared for the metathesis reactions via vapor transport by first grinding and intimately mixing 250 mg (1.78 mmol) of "as-prepared" ZrNCl and 50 mg (0.935 mmol) of dry, sublimed  $\text{NH}_4\text{Cl}$ . This mixture was loaded into 12 mm  $\times$  250 mm silica tubes in the glovebox and then evacuated and sealed. After heating at  $1\text{ }^\circ\text{C min}^{-1}$  to  $800\text{ }^\circ\text{C}$  and holding at that temperature for 2 days, the tube was opened in the glovebox. The crystalline material, which had been transported to the center of the tube (the hottest zone of the furnace), was scraped from the inside walls of the tube.

Typical batches of  $\text{Na}_x\text{ZrNF}_{1+x}$  were prepared by grinding and intimately mixing 200 mg (1.42 mmol) of amorphous or recrystallized ZrNCl and 119 mg (2.84 mmol) of dry NaF. The mixtures were loaded into 9 mm  $\times$  150 mm silica tubes in the glovebox and then evacuated and sealed. A heat gun (approximately  $150\text{ }^\circ\text{C}$ ) was used during evacuation to remove any residual moisture. After heating at  $5\text{ }^\circ\text{C min}^{-1}$  to  $275$  or  $350\text{ }^\circ\text{C}$  (for amorphous and recrystallized ZrNCl reactions, respectively) and holding at that temperature for 5 days, the tube was oven cooled to room temperature and opened in the glovebox. For samples made with the amorphous ZrNCl, the contents were washed and dried as described below. For samples made with recrystallized ZrNCl, the contents were once again ground and intimately mixed with 119 mg (2.84 mmol) of predried NaF in the glovebox. After firing in a silica tube at  $350\text{ }^\circ\text{C}$  for 5 days a second time, the excess sodium halide byproducts were washed away by sonicating with 10 mL of distilled water five times. The product was dried in a  $150\text{ }^\circ\text{C}$  oven, and stored on the benchtop.

$\text{K}_x\text{ZrNF}_{1+x}$  was prepared in a fashion similar to the Na analogue. In this reaction, 176 mg (1.25 mmol) of recrystallized ZrNCl was ground and intimately mixed with 145 mg (2.50 mmol) of dry KF. This reaction mixture was fired in an evacuated, sealed, silica tube at  $275\text{ }^\circ\text{C}$  for 5 days. Two additional grinding/heating cycles ( $275\text{ }^\circ\text{C}$  for 5 days) were completed before washing the product with distilled water and oven drying as described above. Before each of the two additional heating cycles, 145 mg of dry KF was ground and mixed with the product mixture in the nitrogen-filled glovebox.

**Characterization.** X-ray diffraction (XRD) patterns were recorded using a Bruker C2 Discover X-ray powder diffractometer with a HiStar area detector and Cu  $K\alpha$  radiation. Six frames were collected with the area detector and merged to give  $2\theta$  scan ranges from  $4^\circ$  to  $90^\circ$ . Powder XRD profiles used for unit cell refinements were taken with a Bruker D8 Advance X-ray powder diffractometer with a Sol-X detector and Cu  $K\alpha$  radiation from  $4^\circ$  to  $140^\circ$  in  $2\theta$ . High-temperature powder XRD measurements were taken using an Anton Parr heating stage.

Powder neutron diffraction data were collected using the BT-132 detector neutron powder diffractometer at the NCNR, NBSR.

A Cu(311) monochromator with a  $90^\circ$  takeoff angle,  $\lambda = 1.5402$ – $(2)\text{ \AA}$ , and in-pile collimation of 15 min of arc were used. Data were collected over the range of  $3$ – $168^\circ 2\theta$  with a step size of  $0.05^\circ$ . The instrument is described in the NCNR Internet Web site (<http://www.ncnr.nist.gov/>). The sample was sealed in a He environment into a vanadium can sample container of length 50 mm and diameter 6.0 mm. Data were collected under ambient conditions. Unit cell indexing and Rietveld refinements were carried out using MDI Jade, GSAS, and EXPGUI software packages, respectively.<sup>32–34</sup> Rietveld analysis included usable powder neutron diffraction data in the range of  $8$ – $105^\circ 2\theta$ , excluding the low-angle data due to increased background and the high-angle data for lack of discernible peaks.

Energy-dispersive X-ray spectrometry (EDX) was performed with an AMRAY 1820K scanning electron microscope with an acceleration potential of 20 kV. Wavelength-dispersive spectrometry (WDS) was carried out with a JXA-8900 Superprobe, using calcium fluoride ( $\text{CaF}_2$ ), zirconium silicate ( $\text{ZrSiO}_4$ ), and albite ( $\text{NaAlSi}_3\text{O}_8$ ) standards. Secondary standards were used to ensure corrected raw X-ray intensities using CIT-ZAF were accurate, and included topaz ( $\text{Al}_2\text{SiO}_4\text{F}_2$ ), sellaite ( $\text{MgF}_2$ ), and badelleleyite ( $\text{ZrO}_2$ ). Samples and standards were mounted into casting resin epoxy plugs. Compound formulas were calculated from WDS data with reported errors generated from propagated counting statistics. Measurements were made in seven spots for each sample. Zirconium values were normalized to 1.0 for final sample formulas.

Transmission electron micrographs (TEM) and electron diffraction patterns were recorded with a Zeiss EM 10CA transmission electron microscope at 80 kV and a Hitachi Model H-7600 at 110 kV. Samples were loaded onto copper grids by dispersion in water followed by placing a drop of water containing the suspended sample onto the grid and evaporating to dryness.

**Acknowledgment.** We acknowledge the support of the National Institute of Standards and Technology, U.S. Department of Commerce, in providing the neutron research facilities used in this work. Certain commercial products are identified to document experimental procedures. Such identification is not intended to imply recommendation or endorsement by the National Institute of Standards and Technology, nor is it intended to imply that these products are necessarily the best available for the purpose. We are also grateful to the NSF-DMR for support of this work. We are grateful to Tim Mangel (UMCP) and Kevin McIlwrath (Hitachi) for the TEM images.

**Supporting Information Available:** Figures S-1 to S-3 showing structures of  $\text{Na}_x\text{ZrNF}_{1+x}$ , ZrNCl, and related compounds in this paper. This material is available free of charge via the Internet at <http://pubs.acs.org>.

CM051018H

(32) Materials Data, Inc., Livermore, CA, 1999.

(33) Larson, A. C. a. V. D.; R. B. Los Alamos National Laboratory Report LAUR 86-748; 2000.

(34) Toby, B. H. *J. Appl. Crystallogr.* **2001**, *34*, 210–213.